Structure of narrow-diameter single-wall carbon nanotubes grown in $AlPO_4$-5 zeolite

T. Roussel, R. J.-M. Pellenq, and C. Bichara
CRMCN-CNRS and Aix-Marseille Universities, Campus de Luminy, Case 913, F13288 Marseille, France
(Received 29 June 2007; revised manuscript received 18 September 2007; published 18 December 2007)

We present a grand canonical Monte Carlo simulation study of carbon adsorption in $AlPO_4$-5 (AFI) zeolite. An order *N* simplified tight binding model is used for carbon-carbon interactions, and the carbon-matrix interaction is assumed to be weak in the physisorption range. Comparing the almost perfect tubes formed in smooth cylindrical channels and those numerically grown in AFI, we can assess the role of the carbon-wall interaction. In AFI, we obtain defective single-wall nanotubes with a diameter of ≈4 Å, in good agreement with experiments. The tube is thermally stable and presents a mixture of different chiral patterns. The energy cost associated with the defects is about 0.15 eV/atom, indicating that the probability of obtaining defective tubes, with portions of different chiralities along the same zeolite channel, is large.

DOI: 10.1103/PhysRevB.76.235418 PACS number(s): 61.46.Fg, 61.43.Bn, 61.43.Gt

Classically, zeolites are used in heterogeneous catalysis and gas separation. They are now used as a template for preparing metallic or semiconducting nanostructures (clusters, nanowires, and nanotubes).[1] After removal of the zeolite matrix (using acid leaching for instance), these nanostructures are expected to display interesting electronic, optical, or gas storage properties. Among all available zeolite structures, those with a neutral framework are of particular interest since the adsorbed species interact only weakly with the matrix and the electronic structure of the guest can reasonably be assumed to be unaffected by the neighboring host atoms and then results from the geometry of the guest structure only. Two leading examples of such structures are silicalite, a purely siliceous structure, and $AlPO_4$-5. In the case of silicalite, the porous network is made of ≈5 Å straight pores that run in one direction, interconnected perpendicularly with sinusoidal ≈5 Å pores. In contrast, $AlPO_4$-5 presents only parallel channels of ≈7 Å in diameter. Extensive selenium adsorption simulations were performed in the porosity of silicalite and $AlPO_4$-5 (Refs. 2–5) in relation to experimental work,[6–9] paving the way for the simulations described here. $AlPO_4$-5 zeolite, also denoted AFI, was used to produce ultrasmall single-wall carbon nanotubes (SWCNTs) with a diameter of ≈4 Å,[10] which were extensively characterized using high resolution transmission electron microscopy,[11] x-ray scattering,[12,13] micro-Raman measurements,[14,15] polarized absorption spectra,[16–20] photoluminescence spectroscopy,[21] or superconductivity measurements.[22] Once the stability of individual or bundled tubes after matrix removal has been demonstrated, a controversy has appeared concerning the size and chirality of the tubes. Experimental measurements performed on confined tubes exhibit a mixture of the characteristic signatures of tubes of ≈4 Å diameter of different chiralities: armchair (3, 3), chiral (4, 2), and zigzag (5, 0) or (6, 0). This mixture can result either from an averaging over individual perfect tubes in each channel, but different from one channel to the other, or from intrinsically defective tubes. In this paper, we present computer simulations showing that tubes grown in AFI are intrinsically defective, thus helping to solve the controversy.

Up to now, atomistic simulation studies considered only perfect SWCNT's geometrically obtained by rolling up a graphene sheet, freestanding or inside the zeolite porosity. A large amount of work has been devoted to the calculation of their electronic[23–25] or optical properties.[26,27] The relative stability of perfect small diameter SWCNT's was also discussed,[28,29] leading to the conclusion that the total energy differences between the tubes of diameter close to 4 Å are quite small, ruling out a possible selectivity based on the total energy of isolated tubes. In this work, we take the more realistic approach to simulate directly the formation of carbon structures inside the porous matrix. We present a series of grand canonical Monte Carlo (GCMC) simulation results of carbon adsorption in perfectly smooth hollow cylinders with hard repulsive wall and in $AlPO_4$-5. We address both the structure (defects and chirality) and stability of carbon nanostructures in such confining environments. In agreement with the first principles calculations of Dubay and Kresse,[29] the interaction of carbon with the atoms of the zeolite framework is assumed to remain weak in the physisorption energy range. To calculate it, we used a two-body form of the original PN-type potential function.[30] It is based on the usual partition of the adsorption intermolecular energy restricted to two-body terms only: it includes a dispersion interaction term, an induction term, and an empirical repulsive short range contribution. The dispersion term was shown[31] to depend on the atomic polarizabilities and on an effective number of polarizable electrons of all interacting species. The induction term arises from the coupling of the polarizable electronic cloud of the adsorbate, with the electric field induced by the charges carried by the framework species that result from the ionocovalent nature of the matrix itself. The carbon-carbon interaction is described in a tight binding approximation. The total energy is a sum of local (atomic) terms. These include a quantum based attractive band structure term and an empirical repulsive term. We use a minimal s, p_x, p_y, and p_z atomic orbital basis set and a Slater-Koster parametrization to build the Hamiltonian matrix describing the interaction. To describe the total energy as a sum of local terms and to avoid the time consuming diagonalization of the Hamiltonian matrix, which are necessary conditions for an efficient implementation in a Monte Carlo code, we use the recursion method to calculate the local density of electronic states on each atom. We restrict the continued fraction expansion at the fourth moment's level, which means that only first and second neighbors of each site (defined by a cutoff

distance at 2.7 Å) are taken into account to calculate the band energy term. This approximation captures both the quantum nature and the directionality of the bonding. The parameters of the band structure term are those of Xu *et al.*,[32] and the remaining parameters (repulsive term) were fitted against experimental and *ab initio* data.[33] The different hybridization states of C, the elastic constants of the corresponding crystalline phases, and the energy barriers corresponding to the rhombohedral graphite to diamond and to a Stone-Wales transformation are well reproduced.

To check the validity of our approach and to search for optimal conditions to grow tubes, GCMC calculations were first performed in perfect cylinders with hard repulsive walls and dimensions corresponding to the perfect tubes we wished to produce. A minimum of 5×10^5 Monte Carlo macrosteps were performed for each value of the chemical potential, each macrostep consisting of randomly performing 1000 attempted displacements and 100 attempted C insertion and C removals. Starting with a C_2 dimer, we gradually raised the chemical potential of carbon (μ_C), monitored the number of adsorbed C atoms, and analyzed the structures obtained. As soon as the chemical potential of C was large enough, but lower than −5.0 eV/atom, we systematically obtained hollow, more or less defective, carbon structures. The values of μ_C that lead to the best tubes, minimizing the number of defects, vary between −7.5 and −6.0 eV/atom, depending on the temperature. These values are referred to a fictitious monatomic ideal carbon gas and are, therefore, of the same order of magnitude as the energy of formation of the tubes. Low temperatures, below 1500 K, generally led to defective structures, while at higher temperatures (3000 K), perfect structures containing only hexagons were obtained. As expected, the smooth cylinder with a diameter $D=4.15$ Å and a length $L=22.56$ Å led to a (4, 2) nanotube, that with $D=3.92$ Å and $L=25.56$ Å led to a (5, 0) tube, and that with $D=4.07$ Å and $L=24.60$ Å led to a (3, 3) tube. This indicates that our approach is valid, but shows that the finite time of the computer simulation does not always enable one to reach an equilibrium at low temperature. We will, therefore, have to synthesize numerically the tubes at temperatures higher than the experimental ones to obtain realistic structures. The reason for this is that, although Monte Carlo simulations are not bound to follow the real physical time and growth mode, the energy barriers that have to be overcome to heal the defects created during the growth of the samples are of the same order of magnitude as the real ones. Let us recall that, in real life, the graphitization of amorphous carbon takes place at temperatures above 2800 K.

We then tackled the more realistic case of the tube synthesis inside AFI. Switching on the zeolite wall interaction term, we performed GCMC simulations using a periodic box containing five $AlPO_4$-5 orthorhombic unit cells stacked along the pore axis (total length of 42 Å). At $\mu_C=-6.00$ eV/atom and 1000 K, highly defective tubular structures were formed. This temperature corresponds to the actual experimental temperature.[34] Neither amorphous C nor capped tube structures were ever formed. In the experiments of Wang *et al.*,[10] the system was heated for 3 h at various temperatures ranging from 613 to 1073 K, and amorphous carbon structures were obtained for temperature below 773 K. This difference between simulation and experiment can be easily explained considering that, in our simulation, the carbon tube is built atom by atom and that the diffusion of atomic species is not an issue since C atoms are created in the structure, while experiments are done by calcination of complex organic species. Although the GCMC simulations tend to produce a set of configurations at (or close to) thermodynamic equilibrium, we emphasize the fact that we do not mimic the experimental chemical cracking because many aspects of the process (chemical decomposition reaction, kinetics, diffusion, etc.) are bypassed. However, the time scale spanned by the computer simulation is orders of magnitude smaller than the actual time of the experiments. Therefore, in order to heal the defects by overcoming the energy barriers associated with this process, we heated the sample under the same chemical potential conditions up to 3000 K for another complete GCMC run. The resulting structure, denoted as sample 1 in the following, was then fully relaxed.

We first compare the energy of the in-AFI-grown tube (sample 1) and the energies of perfect (m,n) tubes with diameters close to 4 Å [armchair (3, 3), zigzag (5, 0) or (6, 0), and chiral (4, 2)]. These latter tubes have been set inside the AFI by hand and the carbon structure has been relaxed. We also calculated the energies of these tubes after relaxation out of the zeolite. The energies were calculated using the same interaction model and the results are shown in Table I. Let us recall that within our carbon model, the energy of an infinite graphene layer is −7.42 eV/atom.

From Table I, one can see that sample 1 is slightly less stable than (4, 2), (3, 3), and (5, 0) perfect tubes confined in AFI. The largest energy difference is 0.13 eV/atom (about 1500 K, in temperature units). We also note that, contrary to the density functional theory (DFT) calculations of Dubay and Kresse,[29] the (6, 0) tube is significantly less stable than others because the tube zeolite energy is positive (+0.83 eV/atom), meaning that the tube diameter is too large for the space available in the zeolite channel. These DFT results, using either local density approximation or generalized gradient approximation, should certainly be more accurate than the model we use, but seem somewhat surprising since they assign almost the same stability to (5, 0) and (8, 0) tubes inside the zeolite. We can assume that the smaller diameter of the former, resulting in an easier fit in the pore, is compensated by the larger energy cost of its extreme curvature, but it is more difficult to assume that an (8, 0) tube of 6.27 Å diameter can fit inside a pore of 7.3 Å diameter (from one oxygen atom center to the opposite one) without generating a strong repulsive energy. Because of its defective structure, the tube grown by GCMC calculations (sample 1) is less stable than the perfect tubes: its carbon-carbon energy contribution is −6.99, about 0.15 eV/atom less stable than the other, perfect tubes. However, sample 1 finds a slightly better configuration as far as the interaction with the wall is concerned (energy gain ≈0.03eV/atom). This stability analysis indicates that only tubes with a diameter around 4 Å are stable in the channels of the AFI zeolite. This is in agreement with the Raman scattering results in which the radial breathing modes were assigned to tubular structures with this diameter.[14,15]

In order to assess the effect of the corrugation of the

TABLE I. Diameter and energies (confined and freestanding) of selected perfect tubes and the GCMC grown tube. All energies are in eV/atom.

	Tube type				
	(4, 2)	(3, 3)	(5, 0)	(6, 0)	Sample 1
Diameter (Å)	4.15	4.07	3.92	4.70	≈4.0
Energy confined	−7.17	−7.18	−7.17	−6.14	−7.05
C-C energy	−7.14	−7.14	−7.12	−5.32	−6.99
C-zeolite energy	−0.03	−0.04	−0.05	+0.83	−0.07
Energy freestanding	−7.15	−7.15	−7.12	−7.20	−6.99

zeolite-wall interaction potential, we did the same calculations as for sample 1 in smooth hard-walled tubes of the same length (42 Å), with diameters of 4.2 and 4.0 Å. This produced contrasted results in the smooth channels and in the AFI. As shown in Fig. 1, the 4.0 Å diameter tube (denoted sample 3) was almost perfect, the 4.2 Å diameter tube (denoted sample 2) presented a small number of defects, and the in-AFI-grown tube (sample 1) presented a larger number of defects. The number of C atoms per tube for samples 1, 2, and 3 are respectively 180, 176, and 172. All carbon atoms have three neighbors, except for six atoms in sample 1 and one atom in sample 2 that are twofold coordinated. To analyze the structures formed in a quantitative way, we count the numbers of edges of the carbon rings forming the tubes of samples 1–3. The results are summarized in Table II.

In spite of the care we took in obtaining the most ordered structure, sample 1 is clearly defective, with only 70% of the rings being hexagons. Sample 3 is perfect, formed only of hexagons. It displays a (4, 2) chirality and is constrained by the 4 Å diameter and the 42 Å period along its axis. Because of these constraints, the C-C bonds are slightly elongated, by about 1.4%. This is the reason why the number of atoms is smaller than the expected ≈200 atoms for a (4, 2) tube of this length. It also explains why it is 0.15 eV/atom less stable than the perfect (4, 2) tube obtained when the smooth cylinder length perfectly matches the period of the tube. Quite interestingly, sample 2, which has been grown in the same way as sample 3, is defective with 86% hexagons only. We can identify different chiralities on different parts of the tube: (4, 2), (4, 1), and (5, 0) sections are present. These defects could only be removed by running another complete GCMC run at 4000 K.

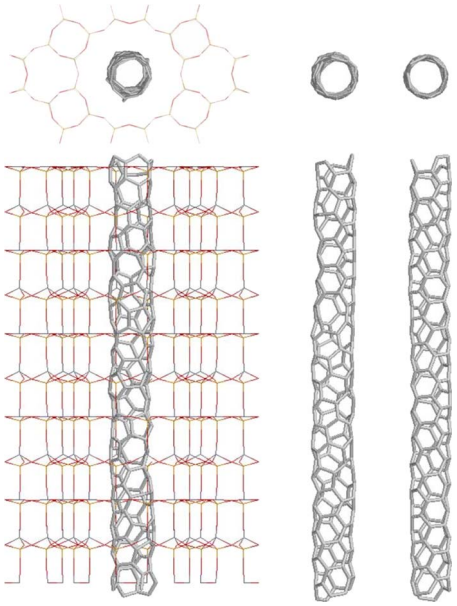

FIG. 1. (Color online) Tubes grown in AFI (left, sample 1), in 4.2 Å (center, sample 2), and in 4 Å (right, sample 3) smooth cylindrical channels.

The radius distribution of tubes 1–3, calculated by averaging 100 stable configurations at 300 K, is shown in Fig. 2. It first shows that no tube with a diameter significantly smaller than 4.0 Å (e.g., 3.0 Å as proposed by Zhao *et al.*[35]) was ever formed. While the radius distribution of tube 3, which is almost perfect, is sharply peaked around 1.83 Å, that of tube 2 tends to be slightly bimodal with peaks at 1.85 and 2.00 Å, and that of sample 1 spreads over the (1.50–2.50) radius range.

These results can be interpreted as follows. The structure of the tubes grown using our GCMC calculations results from two conflicting requirements. First, during their growth, the carbon structures tend to minimize the energy cost of the curvature by occupying as much space as possible. The energy difference between a flat graphene layer and the tubes

TABLE II. Distribution of carbon ring types and carbon-carbon interaction energy of the tubes grown in AFI (sample 1), in 4.2 Å (sample 2), and in 4.0 Å (sample 3) smooth cylindrical channels.

	Sample 1	Sample 2	Sample 3
Number of C	180	176	172
Pentagons	12	5	0
Hexagons	58	74	86
Heptagons	11	7	0
Octagons	5	1	0
Energy (eV/atom)	−6.99	−7.06	−7.03

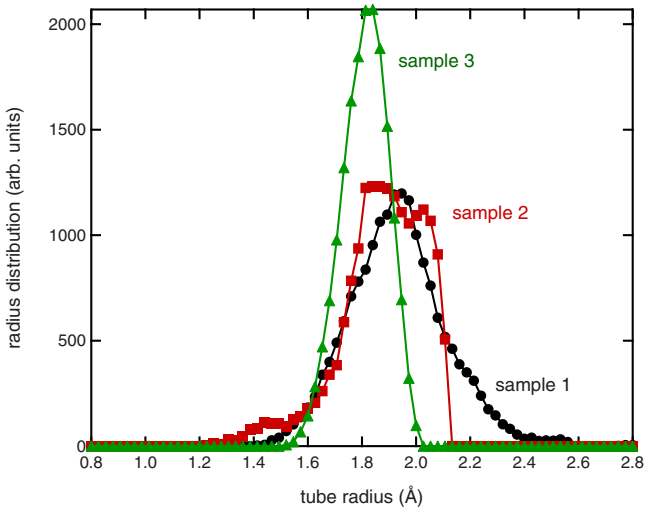

FIG. 2. (Color online) Radius distribution of samples 1 (black), 2 (red), and 3 (green).

compatible with the pores of AFI ranges from 0.27 eV/atom [for a (3, 3) tube] to 0.43 eV/atom (for sample 1). This is the reason why no regular tube with a diameter significantly smaller than 3.60 Å was ever obtained in the simulations. Similar calculations performed in the smaller pores of silicalite never led to any tubular structure. This sets a lower pore diameter limit for the tube formation at ≈5 Å. Second, it appears that the tubes are strongly constrained by the boundary conditions. If these conditions (i.e., the available length and diameter) are compatible with a perfect tube, as in our preliminary tests of the method, defectless tubes are grown. If they are not, as in the case of the in-AFI-grown tube (sample 1) and of sample 3, defective structures are formed. In the strongly optimized structures that were produced, most carbon atoms have three neighbors and bond angles close to 120°. The defects that are formed consist of five-, seven-, and eight-membered rings and the associated energy cost is typically in the 0.15 eV/atom energy range. When the temperature of the computer simulations is lower than 1500 K, the defects that are created during the growth are never healed because the system is trapped in a local energy minimum. At 3000 K, the system has access to a larger portion of the configurational space, and defects can be healed more efficiently, giving rise to perfect structures when possible. Our simulations show that this healing procedure is never effective in the case of sample 1, which is grown in the corrugated energy landscape of the carbon-zeolite interaction. Defects are, therefore, intrinsically present in the form of nonhexagonal rings. The number and arrangement of these defects result from a global (free) energy minimization. In the strongly radially constrained tubes, as, e.g., sample 3, the degeneracy is small and a perfect tube is grown. This example shows that the radial constraint is

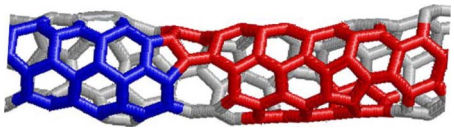

FIG. 3. (Color online) A relaxed in-$AlPO_4$-5-grown tube.

dominant since sample 3 is perfect in spite of a significant mismatch between the period of a perfect (4, 2) tube (unit cell z axis 11.2 Å) and the available 42 Å z axis in the simulation. When the available diameter is larger, as in samples 1 and 2, the degeneracy is larger and defects are present. This is shown in Fig. 3, where small portions of perfect tubes (in red and blue) are linked by defective portions.

The electronic structure of the defective tube obtained in AFI has been calculated using the tight binding model of Xu *et al.*[32] and also using the same orthogonal tight binding model as used by Popov and Henrard[36] to calculate the electronic structure and optical properties of (5, 0), (4, 2), and (3, 3) tubes. Both calculations show a tendency to narrowing or closing the band gap at the Fermi level. However, a full investigation of the electronic properties of the obtained defective tube is difficult because of the large number of atoms in the unit cell and of the lack of symmetries due to the defects. It is beyond the scope of this paper.

This study can be summarized as follows. We have presented a GCMC simulation study of carbon adsorption in the porosity of $AlPO_4$-5 and silicalite zeolites based on a tight binding model for carbon-carbon interactions and a physisorption potential for carbon-zeolite. We found that single-wall nanotubes with a diameter close to 4.0 Å can be grown inside the channels of $AlPO_4$-5 in agreement with experiment. The extreme curvature does not impede carbon atoms to fit the shape of $AlPO_4$-5 channels and form hollow tubular sp^2 nanostructures. Comparing with tubes formed in smooth hard-walled pores of comparable diameters, we found evidence that in-$AlPO_4$-5-grown tubes can be defective with a small energy cost, and demonstrated the crucial role of the corrugation of the carbon-zeolite potential energy surface in the formation of these defects. We further show that inside a single $AlPO_4$-5 pore, patterns with different chiralities can coexist: we present an in-AFI-grown SWCNT that exhibits a mixture of armchair and chiral patterns. Because of the finite simulation time, the number of defects obtained is probably too large. However, our demonstration that tubes with different chiralities can coexist inside one pore of $AlPO_4$-5 sheds a different light on the interpretation of the experimental data. Finally, in the case of silicalite that has smaller pores than $AlPO_4$-5, we obtained a mesh of intercrossing chains showing a lower pore size limit to produce sp^2 carbon nanostructures. This numerical approach to carbon nanocasting by porous materials can be easily transferred to other zeolites such as the three-dimensional interconnected faujasite that should exhibit interesting mechanical or gas storage properties.

[1] S. Qiu, W. Pang, H. Kessler, and J. Guth, Zeolites **9**, 440 (1989).
[2] C. Bichara, R. J.-M. Pellenq, and J.-Y. Raty, Phys. Rev. Lett. **89**, 016101 (2002).
[3] C. Bichara and R. J.-M. Pellenq, Mol. Simul. **30**, 601 (2004).
[4] C. Bichara, J.-Y. Raty, and R. J.-M. Pellenq, Mol. Simul. **30**, 781 (2004).
[5] T. Roussel, C. Bichara, and R. J.-M. Pellenq, Adsorption **11**, 709 (2005).
[6] P. Armand, M.-L. Saboungi, D. L. Price, L. Iton, C. Cramer, and M. Grimsditch, Phys. Rev. Lett. **79**, 2061 (1997).
[7] H. D. Sun, Z. K. Tang, W. M. Zhao, and G. K. L. Wong, Appl. Phys. Lett. **71**, 2457 (1997).
[8] V. V. Poborchii, A. V. Kolobov, J. Caro, V. V. Zhuravlev, and K. Tanaka, Phys. Rev. Lett. **82**, 1955 (1999).
[9] I. L. Li, P. Launois, and Z. K. Tang, Appl. Surf. Sci. **226**, 36 (2004).
[10] N. Wang, Z. K. Tang, G. D. Li, and J. S. Chen, Nature (London) **408**, 50 (2000).
[11] G. D. Li, Z. K. Tang, J. S. Chen, and N. Wang, Carbon **40**, 917 (2002).
[12] P. Launois, R. Moret, D. Le Bolloc'h, P. A. Albouy, Z. K. Tang, G. Li, and J. Chen, Solid State Commun. **116**, 99 (2001).
[13] A. Jorio, A. G. Souza Filho, G. Dresselhaus, M. S. Dresselhaus, A. Righi, F. M. Matinaga, M. S. S. Dantas, M. A. Pimenta, J. Mandes Filho, Z. M. Li, Z. K. Tang, and R. Saito, Chem. Phys. Lett. **351**, 27 (2002).
[14] M. Hulman, H. Kuzmany, O. Dubay, G. Kresse, L. Li, and Z. K. Tang, J. Chem. Phys. **119**, 3384 (2003).
[15] Z. M. Li, Z. K. Tang, G. G. Siu, and I. Bozovic, Appl. Phys. Lett. **84**, 4101 (2004).
[16] Z. M. Li, Z. K. Tang, H. J. Liu, N. Wang, C. T. Chan, R. Saito, S. Okada, G. D. Li, J. S. Chen, N. Nagasawa, and S. Tsuda, Phys. Rev. Lett. **87**, 127401 (2001).
[17] N. Nagasawa, H. Sugiyama, N. Naka, I. Kudryashov, M. Watanabe, T. Hayashi, I. Bozovic, N. Bozovic, G. Li, Z. Li, and Z. K. Tang, J. Lumin. **97**, 161 (2002).
[18] W. Liang, G. Chen, Z. Li, and Z. K. Tang, Appl. Phys. Lett. **80**, 3415 (2002).
[19] I. L. Li, G. D. Li, H. J. Liu, C. T. Chen, and Z. K. Tang, Appl. Phys. Lett. **82**, 1467 (2003).
[20] I. L. Li and Z. K. Tang, Appl. Surf. Sci. **226**, 72 (2004).
[21] J. Guo, C. Yang, Z. M. Li, M. Bai, H. J. Liu, G. D. Li, E. G. Wang, C. T. Chan, Z. K. Tang, W. K. Ge, and X. Xiao, Phys. Rev. Lett. **93**, 017402 (2004).
[22] Z. K. Tang, Z. L. Zhang, N. Wang, X. Zhang, H. Wen, G. D. Li, J. N. Wang, C. T. Chan, and P. Sheng, Science **292**, 2462 (2001).
[23] X. Blase, L. X. Benedict, E. L. Shirley, and S. G. Louie, Phys. Rev. Lett. **72**, 1878 (1994).
[24] V. Zolyómi and J. Kürti, Phys. Rev. B **70**, 085403 (2004).
[25] D. Connétable, G. M. Rignanese, J. C. Charlier, and X. Blase, Phys. Rev. Lett. **94**, 015503 (2005).
[26] A. G. Marinopoulos, L. Reining, A. Rubio, and N. Vast, Phys. Rev. Lett. **91**, 046402 (2003).
[27] M. Machón, S. Reich, C. Thomsen, D. Sánchez-Portal, and P. Ordejón, Phys. Rev. B **66**, 155410 (2002).
[28] L. M. Peng, Z. L. Zhang, Z. Q. Xue, Q. D. Wu., Z. N. Gu, and D. G. Pettifor, Phys. Rev. Lett. **85**, 3249 (2000).
[29] O. Dubay and G. Kresse, Carbon **42**, 979 (2004).
[30] R. J.-M. Pellenq and D. Nicholson, J. Phys. Chem. **98**, 13339 (1994).
[31] R. J.-M. Pellenq and D. Nicholson, Mol. Phys. **95**, 549 (1998).
[32] C. H. Xu, C. Z. Wang, C. T. Chan, and K. M. Ho, J. Phys.: Condens. Matter **4**, 6047 (1992).
[33] H. Amara, Ch. Bichara, and F. Ducastelle, Phys. Rev. B **73**, 113404 (2006); H. Amara, Ph.D. thesis, Université Paris VI, 2005, available at http://lem.onera.fr/Theses.html
[34] Z. K. Tang, N. Wang, X. X. Zhang, J. N. Wang, C. T. Chan, and P. Sheng, New J. Phys. **146**, 1 (2003).
[35] X. Zhao, Y. Liu, S. Inoue, T. Suzuki, R. O. Jones, and Y. Ando, Phys. Rev. Lett. **92**, 125502 (2004).
[36] V. N. Popov and L. Henrard, Phys. Rev. B **70**, 115407 (2004).